HHS Public Access

Author manuscript

J Fluor Chem. Author manuscript; available in PMC 2022 May 01.

Published in final edited form as:

J Fluor Chem. 2021 May ; 245: . doi:10.1016/j.jfluchem.2021.109760.

Radiofluorination of oxazole-carboxamides for preclinical PET neuroimaging of GSK-3

Cassis Varlow[a,b,†], **Andrew V. Mossine**[c,†], **Vadim Bernard-Gauthier**[a], **Peter J. H. Scott**[c,*], **Neil Vasdev**[a,b,*]

[a]Azrieli Centre for Neuro-Radiochemistry, Brain Health Imaging Centre, Centre for Addiction and Mental Health, Toronto, ON, M5T 1R8, Canada

[b]Institute of Medical Science, University of Toronto, Toronto, ON, M5T 1R8, Canada

[c]Department of Radiology, University of Michigan Medical School, Ann Arbor, MI 48109, United States

Abstract

Glycogen synthase kinase 3 (GSK-3) is an enzyme that is dysregulated in oncology neurodegeneration, neuroinflammation and several mental health illnesses. As such, GSK-3 is a long-sought after target for positron emission tomography (PET) imaging and therapeutic intervention. Herein, we report on the development and radiofluorination of two oxazole-4-carboxamides, including one bearing a non-activated aromatic ring. Both compounds demonstrated excellent selectivity in a kinase screen and inhibit GSK-3 with high affinity. [^{18}F]OCM-49 was synthesized from [^{18}F]fluoride using a copper-mediated reaction of an aryl boronic acid precursor, while [^{18}F]OCM-50 used a trimethylammonium triflate precursor, and both radiotracers were translated for preclinical PET imaging in rodents. Due to superior radiochemical yields and brain uptake (peak standardized uptake value of ~2.0), [^{18}F]OCM-50 was further evaluated in non-human primate and also showed good brain uptake and rapid clearance. Further studies to consider clinical translation of both radiotracers are underway.

Graphical Abstract

[*]**Corresponding Authors:** Peter J. H. Scott, Ph.D., Phone: 734-615-1756, pjhscott@umich.edu, Department of Radiology, University of Michigan, 1301 Catherine St., Ann Arbor, Michigan 48109, United States, Neil Vasdev, Ph.D., neil.vasdev@utoronto.ca, Phone: 416-535-8501, ext. 30988, Brain Health Imaging Center, Centre for Addiction and Mental Health, 250 College St., Toronto, ON., M5T 1R8, Canada.

[†]co-first author

Declaration of interests

The authors declare that they have no known competing financial interests or personal relationships that could have appeared to influence the work reported in this paper.

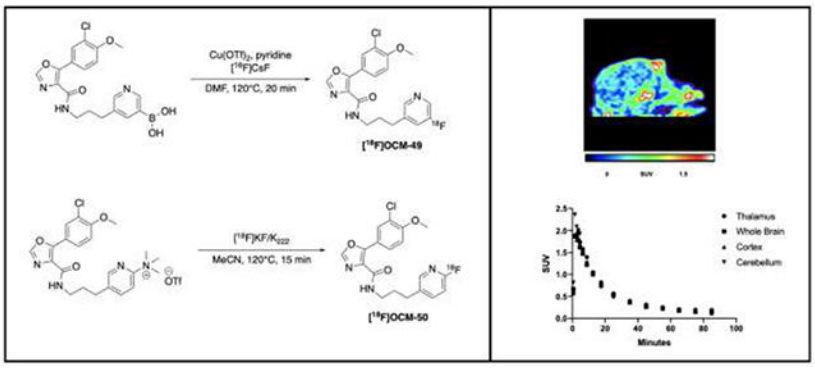

Keywords

glycogen synthase kinase 3; GSK-3; fluorine-18; PET imaging; copper-mediated radiofluorination; neuroimaging

1. Introduction

Glycogen synthase kinase 3 (GSK-3) is a serine/threonine kinase that is highly abundant and globally expressed in the central nervous system (CNS). GSK-3 exists as two isoforms: GSK-3α and GSK-3β and is involved in several signal transduction pathways that contribute to the regulation of differentiation as well as development, metabolism, cell cycle regulation, and neuroprotection [1–5]. GSK-3α/β dysregulation has been explored in oncology (WNT pathway) as well as in mental health illnesses, including bipolar disorder as GSK-3 is the target of the therapeutic, lithium [6]. Dysregulation of GSK-3β activity has also been proposed in the pathogenesis of neurodegenerative diseases such as Alzheimer's disease (AD), Huntington's disease (HD) and Parkinson's disease (PD) [5]. A "GSK-3 hypothesis of AD" has been proposed, as increased kinase activity may contribute to hyperphosphorylation of tau protein and the subsequent formation of neurofibrillary tangles (NFTs), increased amyloid-β production and inflammatory cytokine production in human peripheral immune cells [7–10]. Inhibition of GSK-3 kinase activity is of interest as an AD therapy because it has shown modulation of tau hyperphosphorylation and has potential to prevent the formation of NFTs [11]. Additionally, GSK-3 activity constitutively inhibits neuroprotective signalling pathways and downregulation has been reported following traumatic brain injury (TBI) [12]. These findings have attracted interest to pharmacological GSK-3 inhibition following TBI, with studies showing promise for this therapeutic strategy to reduce tau pathology and neuronal death [13]. Aberrant GSK-3 activity has been extensively linked to neurodegeneration, psychiatric disorders, TBI and several cancers. There have been longstanding efforts to develop positron emission tomography (PET) radiotracers for *in vivo* imaging of GSK-3. PET imaging allows for monitoring and diagnosis of diseases and disorders, patient selection for clinical trials, and in drug discovery by enabling pharmacokinetic studies, confirming target engagement and dosing regimens [2, 14].

In 2004, our laboratories in Toronto reported the first GSK-3 targeting radiotracer labeled with carbon-11 (^{11}C; $t_{1/2}$ = 20.3 min), [^{11}C]AR-A014418, and have continued efforts to develop a GSK-3 tracer for first-in-human imaging. Our laboratories in Michigan subsequently developed the first brain penetrant GSK-3 radiotracer ([^{11}C]SB-216763) [15, 16]. We have since shifted our efforts to a new series of GSK-3 targeting radiotracers based on the oxazole-4-carboxamide structural scaffold and identified [^{11}C]PF-367 [16] as one of the most potent and selective GSK-3 inhibitors. Together, we recently developed PF-367 analogues labeled with carbon-11, such as [^{11}C]OCM-44 [17, 18]. To date, there is only one report of a fluorine-18 (^{18}F; $t_{1/2}$ = 109.7 min) labeled PET tracer for GSK-3 (the maleimide radiotracer [^{18}F]10a; Fig 1), however, moderate brain uptake in rodents and lack of saturable binding precluded its further use [19]. Efforts toward development and translation of GSK-3 radiotracers for human imaging are ongoing [20–24] and reported PET tracers for GSK-3 are depicted in Figure 1.

As seen in Figure 1, the vast majority of GSK-3 targeting radiotracers reported have been radiolabeled with carbon-11. The longer half-life of ^{18}F radionuclide allows for extended imaging protocols, which often provide a better indication of the pharmacokinetics, as well as off-site manufacture and shipping of radiotracers to locations that may not be fully equipped with cyclotron and radiochemistry production facilities, thereby enabling multi-center clinical trials. Despite fluorine-18 being the most commonly used radionuclide for PET imaging, there is only one ^{18}F radiolabeled GSK-3 tracer ([^{18}F]10a) reported to date but is not suitable for *in vivo* neuroimaging of this target (*vide supra*). Our lead fluorinated derivatives of PF-367 with potential to improve upon GSK-3 selectivity, affinity and brain uptake, are identified as OCM-49 and OCM-50 (Figure 1) [18]. These two lead compounds are amenable to labeling with [^{18}F]fluoride at the aromatic ring. However, OCM-49 requires radiofluorination of a non-activated aromatic ring. Such reactions are among the most challenging in the field of radiofluorination as noted in extensive reviews including those from our laboratories [25, 26]. OCM-49 was reported to be selective for GSK-3β with an inhibitory constant (K_i) of 0.36 nM, a central nervous system multiparameter optimization (CNS MPO) score of 4.67/6.0 and an unbound fraction in plasma of 0.04 [22]. OCM-50 was reported GSK-3β selective with a K_i of 0.28 nM, a CNS MPO score of 4.8/6.0 and an unbound fraction in plasma of 0.03 [18, 27]. Due to these favourable physiochemical properties, both compounds were chosen for radiofluorination and evaluation as ^{18}F-labeled PET radiotracers for GSK-3β. In this work, we report additional kinase selectivity data for OCM-49 and OCM-50, the radiofluorination and preclinical evaluation by *in vivo* PET imaging in rodent with both radiotracers, and PET neuroimaging in non-human primate (NHP) with [^{18}F]OCM-50.

2. Results and Discussion

2.1 Kinase Selectivity

Our recent report showed that OCM-49 and OCM-50 have exquisite selectivity by chemical proteomic (KiNativ) profiling using brain lysates (ActivX Bioscience; La Jolla, CA) [19]. Herein, OCM-49 and OCM-50 were further evaluated in a kinase screen (Reaction Biology©), assessing selectivity against 370 recombinant kinases. At an assay concentration

of 1 μM, OCM-49 inhibited 98.97% and 92.50% of GSK-3α and GSK-β activity, respectively. At the same concentration, OCM-50 inhibited 103.84% and 93.46% of GSK-3α and GSK-β, respectively. Of note, both compounds inhibited the kinases DRAK1/STK17A and DYRK1/DYRK1A in the range of 70–80%. Full selectivity data is shown in Supporting Information (SI), Fig. S1.

2.2 [^{18}F]OCM-49 Synthesis

[^{18}F]OCM-49 was synthesized *via* copper-mediated radiofluorination of a boronic acid precursor **(1**; radiofluorination described in Scheme 1). Advantages of radiofluorination of arylboronic acid precursors include stability, as most are crystalline solids with long shelf-lives and can be handled without special precautions [28–30]. Furthermore, arylboronate precursors also enable radiofluorination of arene non-activated sites, such as in [^{18}F]OCM-49. TBAOTf/Cs_2CO_3 was used to elute $^{18}F^-$ from the quaternary methylammonium (QMA) ion exchange cartridge, as elution with K_2CO_3 in the absence of 4,7,13,16,21,24-Hexaoxa-1,10-diazabicyclo[8.8.8]hexacosane (Kryptofix® 222; K2.2.2) leads to poor fluoride solubility in organic media. Furthermore, both K2.2.2. and K_2CO_3 have shown to interfere with copper-mediated radiofluorination, resulting in suppressed yields [31]. [^{18}F]OCM-49 was obtained in a low radiochemical yield (RCY; 0.1%) with a molar activity (*A*m) of 1.081 Ci/μmol (40 GBq/μmol). This RCY was determined insufficient to produce [^{18}F]OCM-49 in suitable quantities for NHP imaging, but sufficient quantities were isolated and formulated for rodent imaging.

2.3 [^{18}F]OCM-50 Synthesis

The trimethylammonium triflate precursor **(2)** was synthesized for [^{18}F]OCM-50, enabling radiotracer synthesis *via* nucleophilic radiofluorination (SNAr) with [^{18}F]fluoride (Scheme 2) [32]. [^{18}F]OCM-50 was obtained in 6.6% RCY with a A_m of 5.941 Ci/μmol (220 GBq/μmol). This RCY produced sufficient quantities of [^{18}F]OCM-50 for preclinical rodent imaging as well as further evaluation in higher species.

2.4 Rodent Imaging

Initial preclinical evaluation of [^{18}F]OCM-49 and [^{18}F]OCM-50 was carried out in Sprague Dawley rats to assess brain penetration and pharmacokinetics in a baseline PET imaging study. A representative summed image of [^{18}F]OCM-49 brain uptake following *i.v.* administration (0.152 mCi, 5.6 MBq) showed uptake and retention of the radiotracer (Fig. 2A). Radioactivity reached a maximum peak uptake of 1.5 standardized uptake value (SUV) and retained below 0.2 after 30 minutes (Fig. 2B). Additionally, rodent imaging was conducted with [^{18}F]OCM-50. A representative summed image showed similar uptake in the rat brain (Fig. 2C) following *i.v.* administration of [^{18}F]OCM-50 (0.405 mCi, 15.0 MBq). Radioactivity reached a maximum peak uptake of 2.0 SUV in whole brain and decreased to below 0.2 after 30 minutes (Fig. 2D). [^{18}F]OCM-50 displayed good brain uptake and retention, with a 2-fold increase in comparison to the parent compound, [^{11}C]PF-367 (peak SUV = 1.0) [18]. Due to the low RCY of [^{18}F]OCM-49 and relatively lower brain uptake compared to [^{18}F]OCM-50, only the latter was advanced for NHP imaging.

2.5 NHP Imaging

[^{18}F]OCM-50 was translated for imaging in NHP, where a baseline PET study was conducted in one female rhesus monkey (Fig. 3A). Following *i.v.* administration of [^{18}F]OCM-50 (4.08 mCi, 150.8 MBq), activity reached a whole brain peak of ~2.0 SUV within the first 2 minutes and retained below 0.4 SUV after 30 minutes of scan time (Fig. 3B). The promising brain uptake and clearance profile of the radiotracer in naïve NHP closely resembled the rodent imaging and, since there was also no evidence of metabolic defluorination, further evaluation of [^{18}F]OCM-50 as a GSK-3 imaging agent in the CNS is warranted.

3 Conclusions

The goal of developing [^{18}F]OCM-49 and [^{18}F]OCM-50 from the parent compound [^{11}C]PF-367, was to improve upon brain penetration, selectivity and affinity for GSK-3, while incorporating all the advantages of the ^{18}F radionuclide. [^{18}F]OCM-49 was synthesized using copper-mediated radiofluorination of a boronic acid precursor, albeit in low RCY. Moderate brain uptake of [^{18}F]OCM-49 was observed, and is comparable to the brain uptake observed with [^{11}C]PF-367. Despite demonstrating uptake in the rodent brain, the low RCY precluded further evaluation of this tracer in NHP at this time. [^{18}F]OCM-50 was synthesized *via* nucleophilic aromatic substitution in RCYs suitable for preclinical evaluation in both rodent and NHP. The results from these imaging studies were closely related, with [^{18}F]OCM-50 displaying good brain uptake, quick washout and retention of the radiotracer throughout the duration of the PET scans. Future work involving these radiotracers includes increasing the RCY for [^{18}F]OCM-49, and will consider design of experiments (DoE) approaches for optimizing the copper-mediated radiofluorination reaction [33], to enable PET imaging studies in higher species, as well as evaluation of both tracers to establish their radiometabolite profiles and to confirm *in vivo* specific binding toward GSK-3.

4 Experimental

4.1 General Radiochemistry

All reagents were purchased commercially from Millipore Sigma, unless otherwise stated. OCM-49 and OCM-50 were synthesized by Sai Life Sciences as previously reported by our laboratories.[18] [^{18}F]Fluoride (~1.8 Ci) was produced via the ^{18}O(p,n)^{18}F nuclear reaction using a (General Electric, GE) GE PETTrace cyclotron. The [^{18}F]fluoride was delivered to the synthesis module (GE TRACERLab FX_{FN}) in a 2.5 mL bolus of [^{18}O]water and trapped on a QMA-light Sep-Pak preconditioned with potassium triflate (10 mL, 0.5 M, [^{18}F]OCM-49) or sodium bicarbonate (10 mL, 0.5 M, [^{18}F]OCM-50) to remove [^{18}O]water and potential cyclotron target-generated impurities. [^{18}F]Fluoride was eluted into the reaction vessel using an aqueous solution of base indicated in each experimental section (4.2 and 4.3 below), see SI for additional details. Acetonitrile (CH_3CN; 1 mL) was added to the reaction vessel, and the resulting solution was dried by azeotropic distillation to provide anhydrous $^{18}F^-$. Azeotropic drying/evaporation was achieved by heating the reaction vessel to 100 °C and drawing vacuum for 6 min. The reaction vessel was then simultaneously

subjected to an argon stream and vacuum draw for an additional 6 min. Anhydrous, air-free solvent was added to the dried reagent, and the sample was cooled to 40 °C for subsequent use in reactions.

4.2 [^{18}F]OCM-49

Precursor (**1,** 1.8 mg, Sai Life Sciences) was dissolved in 1000 μL dimethylformamide (DMF) in the presence of 0.25 μL methanesulfonic acid, 7.2 mg copper(II)trifluoromethanesulfonate and 39.1 μL pyridine. This mixture was added to a V-vial containing azeotropically dried [^{18}F]CsF (500 μL 15mg/mL TBAOTf + 0.2 mg/mL Cs_2CO_3). The reaction was heated at 120 ° C for 20 min. The reaction mixture was cooled to 40 ° C, added 500 μL 0.25 M ascorbic acid and stirred for 1 min. The reaction was then quenched with HPLC mobile phase (45/65 MeCN/10 mM NH_4OAc (pH: 7.3)) and loaded onto HPLC (45/65 MeCN/10 mM NH_4OAc (pH: 7.3) (v/v) isocratic; flow rate: 5.0 mL/min; semipreparative column: Phenomenex Luna C18, 10 μm, 10 × 250 mm, 5 mL/min). The peak was collected (~22.5 – 24.5 min) and diluted with 50 mL water. The solution was transferred through a preconditioned (ethanol (10 mL) and water (10 mL)) Oasis HLB 1cc vac cartridge and the cartridge was then washed with 10 mL water. The radiotracer was eluted with 100 μL EtOH and the cartridge was washed with 1.0 mL 0.9% buffered saline. [^{18}F]OCM-49 product identity confirmed by radio-HPLC co-injection with unlabeled reference standard. Analytical HPLC conditions: 50/50 MeCN/10 mM NH_4OAc (pH: 7.4) (v/v) isocratic; flow rate: 1.0 mL/min; QC column: Phenomenex Luna C18, 5 μm, 4.6 × 150 mm.

4.3 [^{18}F]OCM-50

Precursor **(2,** 1 mg, Sai Life Sciences) was dissolved in dimethyl sulfoxide (Me_2SO, 500 μL) and added azeotropically dried [^{18}F]KF (500 μL 7 mg/mL K_2CO_3 + 1 mL of 15 mg/mL K2.2.2 in acetonitrile). The reaction was heated at 120 ° C for 15 min. The reaction mixture was cooled to 50 ° C and then quenched with HPLC mobile phase (50/50 MeCN/10mM NH_4OAc (pH: 7.3)) loaded onto HPLC (50/50 MeCN/20 mM NH_4OAc (pH: 7.3) (v/v) isocratic; flow rate: 5.0 mL/min; semipreparative column: Phenomenex Luna C18, 10 μm, 10 × 250 mm, 5 mL/min). The peak was collected (~15 – 17 min), diluted with 50 mL H_2O, and the solution was transferred through a preconditioned (ethanol (10 mL) and water (10 mL)) C18 1cc Vac Sep-Pak®. The radiotracer was eluted with 500 μL EtOH. The C18 cartridge was then washed with 4.5 mL buffered saline. [^{18}F]OCM-50 product identity was confirmed by radio-HPLC co-injection with unlabeled reference standard. Analytical HPLC conditions: 50/50 MeCN/10 mM NH_4OAC (pH: 7.3) (v/v) isocratic; flow rate: 1.0 mL/min; QC column: Phenomenex Luna C18, 5 μm, 4.6 × 150 mm.

4.4 Rodent and NHP PET Imaging

Rodent and nonhuman primate PET imaging studies were performed in accordance with the standards set by the Institutional Animal Care and Use Committee (IACUC) at the University of Michigan. Rat imaging was done using Sprague Dawley (body weight = ~325 g). NHP imaging was done using a mature female rhesus monkey (body weight = ~8.7 kg, 15 years of age). PET imaging of [^{18}F]OCM-49 and [^{18}F]OCM-50 was conducted using a

Concorde Microsystems MicroPET P4 tomograph. For rat imaging, animals were anesthetized (isoflurane), and positioned in the PET scanner. Anesthesia was maintained with 2–4% isoflurane/O_2 throughout the imaging studies. Following a transmission scan, the animal was injected (*i.v.* tail vein injection) with the radiotracer ([^{18}F]OCM-49: 5.6 MBq; [^{18}F]OCM-50: 14.8 MBq) as a bolus over 1 min, and the brain imaged for 90 min 4 × 1 min frames – 1 × 1.75 min frames – 1 × 2.5 min frames – 1 × 3.75 min frames – 1 × 5 min frames – 1 × 7.5 min frames - 6 × 10 min frames). For NHP, the animal was anesthetized (ketamine) and intubated, a venous catheter was inserted into one hindlimb and the animal positioned on the bed of the MicroPET gantry. A head-holder was used to prevent motion artifacts. Isoflurane anesthesia was then applied (2–4% isoflurane/O_2) and continued throughout the study. Following a transmission scan, the animal was injected *i.v.* with the radiotracer ([^{18}F]OCM-50: 150.8 MBq) as a bolus over 1 min, and the brain imaged for 90 min (4 × 1 min frames – 1 × 1.75 min frames – 1 × 2.5 min frames – 1 × 3.75 min frames – 1 × 5 min frames – 1 × 7.5 min frames - 6 × 10 min frames). Emission data were corrected for attenuation and scatter and reconstructed using the 3D maximum a priori method (3D MAP algorithm). Using a summed image of the entire data set, regions of interest (ROIs) were drawn manually on multiple planes to obtain volumetric ROIs for the whole brain, thalamus, cortex, and cerebellum. The volumetric ROIs were then applied to the full dynamic data sets to obtain the regional tissue time-radioactivity data.

Supplementary Material

Refer to Web version on PubMed Central for supplementary material.

Acknowledgements:

N.V. thanks National Institute on Ageing of the NIH (R01AG054473), the Azrieli Foundation and the Canada Research Chairs Program, Canada Foundation for Innovation and the Ontario Research Fund for support. P. J. H. S. thanks the DOE (DE-SC0012484) and NIH (R01EB021155) for financial support.

References:

1. Woodgett JR, Molecular cloning and expression of glycogen synthase kinase-3/factor A. The EMBO journal 1990, 9 (8), 2431–2438. [PubMed: 2164470]
2. Pandey MK; DeGrado TR, Glycogen Synthase Kinase-3 (GSK-3)-Targeted Therapy and Imaging. Theranostics 2016, 6 (4), 571–593. [PubMed: 26941849]
3. Jope RS; Johnson GVW, The glamour and gloom of glycogen synthase kinase-3. Trends in Biochemical Sciences 2004, 29 (2), 95–102. [PubMed: 15102436]
4. Meijer L; Flajolet M; Greengard P, Pharmacological inhibitors of glycogen synthase kinase 3. Trends in Pharmacological Sciences 2004, 25 (9), 471–480. [PubMed: 15559249]
5. Lei P; Ayton S; Bush AI; Adlard PA, GSK-3 in Neurodegenerative Diseases. International journal of Alzheimer's disease 2011, 2011, 189246–189246.
6. Jope RS, Lithium and GSK-3: one inhibitor, two inhibitory actions, multiple outcomes. Trends in Pharmacological Sciences 2003, 24 (9), 441–443. [PubMed: 12967765]
7. Martinez A; Perez DI; Gil C, Lessons Learnt from Glycogen Synthase Kinase 3 Inhibitors Development for Alzheimer's Disease. Current Topics in Medicinal Chemistry 2013, 13 (15), 1808–1819. [PubMed: 23931441]
8. Eldar-Finkelman H; Martinez A, GSK-3 Inhibitors: Preclinical and Clinical Focus on CNS. Frontiers in Molecular Neuroscience 2011, 4, 32. [PubMed: 22065134]

9. Hooper C; Killick R; Lovestone S, The GSK3 hypothesis of Alzheimer's disease. Journal of neurochemistry 2008, 104 (6), 1433–1439. [PubMed: 18088381]
10. Martin M; Rehani K; Jope RS; Michalek SM, Toll-like receptor-mediated cytokine production is differentially regulated by glycogen synthase kinase 3. Nature immunology 2005, 6 (8), 777–784. [PubMed: 16007092]
11. Arciniegas MDD; Adler MDL; Topkoff J; Cawthra RNE; Filley MDCM; Reite MDM, Subject Review: Attention and memory dysfunction after traumatic brain injury: cholinergic mechanisms, sensory gating, and a hypothesis for further investigation. Brain Injury 1999, 13 (1), 1–13. [PubMed: 9972437]
12. Hur E-M; Zhou F-Q, GSK3 signalling in neural development. Nature reviews. Neuroscience 2010, 11 (8), 539–551. [PubMed: 20648061]
13. Shim SS; Stutzmann GE, Inhibition of Glycogen Synthase Kinase-3: An Emerging Target in the Treatment of Traumatic Brain Injury. Journal of Neurotrauma 2016, 33 (23), 2065–2076. [PubMed: 26979735]
14. Hicks JW; VanBrocklin HF; Wilson AA; Houle S; Vasdev N, Radiolabeled Small Molecule Protein Kinase Inhibitors for Imaging with PET or SPECT. Molecules 2010, 15, 8260–8278. [PubMed: 21079565]
15. Vasdev N; Garcia A; Stableford WT; Young AB; Meyer JH; Houle S; Wilson AA, Synthesis and ex vivo evaluation of carbon-11 labelled N-(4-methoxybenzyl)-N′-(5-nitro-1,3-thiazol-2-yl)urea ([11C]AR-A014418): A radiolabelled glycogen synthase kinase-3β specific inhibitor for PET studies. Bioorganic & Medicinal Chemistry Letters 2005, 15 (23), 5270–5273. [PubMed: 16202587]
16. Li L; Shao X; Cole EL; Ohnmacht SA; Ferrari V; Hong YT; Williamson DJ; Fryer TD; Quesada CA; Sherman P; Riss PJ; Scott PJH; Aigbirhio FI, Synthesis and Initial in Vivo Studies with [11C]SB-216763: The First Radiolabeled Brain Penetrative Inhibitor of GSK-3. ACS Medicinal Chemistry Letters 2015, 6 (5), 548–552. [PubMed: 26005531]
17. Liang SH; Chen JM; Normandin MD; Chang JS; Chang GC; Taylor CK; Trapa P; Plummer MS; Para KS; Conn EL; Lopresti-Morrow L; Lanyon LF; Cook JM; Richter KEG; Nolan CE; Schachter JB; Janat F; Che Y; Shanmugasundaram V; Lefker BA; Enerson BE; Livni E; Wang L; Guehl NJ; Patnaik D; Wagner FF; Perlis R; Holson EB; Haggarty SJ; El Fakhri G; Kurumbail RG; Vasdev N, Discovery of a Highly Selective Glycogen Synthase Kinase-3 Inhibitor (PF-04802367) That Modulates Tau Phosphorylation in the Brain: Translation for PET Neuroimaging. Angewandte Chemie International Edition 2016, 55 (33), 9601–9605. [PubMed: 27355874]
18. Bernard-Gauthier V; Mossine AV; Knight A; Patnaik D; Zhao W-N; Cheng C; Krishnan HS; Xuan LL; Chindavong PS; Reis SA; Chen JM; Shao X; Stauff J; Arteaga J; Sherman P; Salem N; Bonsall D; Amaral B; Varlow C; Wells L; Martarello L; Patel S; Liang SH; Kurumbail RG; Haggarty SJ; Scott PJH; Vasdev N, Structural Basis for Achieving GSK-3β Inhibition with High Potency, Selectivity, and Brain Exposure for Positron Emission Tomography Imaging and Drug Discovery. Journal of Medicinal Chemistry 2019, 62 (21), 9600–9617. [PubMed: 31535859]
19. Hu K; Patnaik D; Collier TL; Lee KN; Gao H; Swoyer MR; Rotstein BH; Krishnan HS; Liang SH; Wang J; Yan Z; Hooker JM; Vasdev N; Haggarty SJ; Ngai M-Y, Development of [18F]Maleimide-Based Glycogen Synthase Kinase-3β Ligands for Positron Emission Tomography Imaging. ACS Medicinal Chemistry Letters 2017, 8 (3), 287–292. [PubMed: 28337318]
20. Cole EL; Shao X; Sherman P; Quesada C; Fawaz MV; Desmond TJ; Scott PJH, Synthesis and evaluation of [(11)C]PyrATP-1, a novel radiotracer for PET imaging of glycogen synthase kinase-3β (GSK-3β). Nuclear medicine and biology 2014, 41 (6), 507–512. [PubMed: 24768148]
21. Kumata K; Yui J; Xie L; Zhang Y; Nengaki N; Fujinaga M; Yamasaki T; Shimoda Y; Zhang M-R, Radiosynthesis and preliminary PET evaluation of glycogen synthase kinase 3β (GSK-3β) inhibitors containing [11C]methylsulfanyl, [11C]methylsulfinyl or [11C]methylsulfonyl groups. Bioorganic & Medicinal Chemistry Letters 2015, 25 (16), 3230–3233. [PubMed: 26067173]
22. Prabhakaran J; Sai KKS; Sattiraju A; Mintz A; Mann JJ; Kumar JSD, Radiosynthesis and evaluation of [11C]CMP, a high affinity GSK3 ligand. Bioorganic & Medicinal Chemistry Letters 2019, 29 (6), 778–781. [PubMed: 30709652]
23. Prabhakaran J; Zanderigo F; Sai KKS; Rubin-Falcone H; Jorgensen MJ; Kaplan JR; Mintz A; Mann JJ; Kumar JSD, Radiosynthesis and in Vivo Evaluation of [11C]A1070722, a High Affinity

GSK-3 PET Tracer in Primate Brain. ACS Chemical Neuroscience 2017, 8 (8), 1697–1703. [PubMed: 28485573]

24. Mossine AV; Brooks AF; Jackson IM; Quesada CA; Sherman P; Cole EL; Donnelly DJ; Scott PJH; Shao X, Synthesis of Diverse 11C-Labeled PET Radiotracers via Direct Incorporation of [11C]CO2. Bioconjugate Chemistry 2016, 27 (5), 1382–1389. [PubMed: 27043721]
25. Brooks AF; Topczewski JJ; Ichiishi N; Sanford MS; Scott PJH, Late-stage [18F]fluorination: new solutions to old problems. Chemical Science 2014, 5 (12), 4545–4553. [PubMed: 25379166]
26. Deng X; Rong J; Wang L; Vasdev N; Zhang L; Josephson L; Liang SH, Chemistry for Positron Emission Tomography: Recent Advances in 11C-, 18F-, 13N-, and 15O-Labeling Reactions. Angewandte Chemie International Edition 2019, 58 (9), 2580–2605. [PubMed: 30054961]
27. Wager TT; Hou X; Verhoest PR; Villalobos A, Moving beyond rules: the development of a central nervous system multiparameter optimization (CNS MPO) approach to enable alignment of druglike properties. ACS chemical neuroscience 2010, 1 (6), 435–449. [PubMed: 22778837]
28. Mossine AV; Brooks AF; Makaravage KJ; Miller JM; Ichiishi N; Sanford MS; Scott PJH, Synthesis of [18F]Arenes via the Copper-Mediated [18F]Fluorination of Boronic Acids. Organic Letters 2015, 17 (23), 5780–5783. [PubMed: 26568457]
29. Bernard-Gauthier V; Lepage ML; Waengler B; Bailey JJ; Liang SH; Perrin DM; Vasdev N; Schirrmacher R, Recent Advances in 18F Radiochemistry: A Focus on B-18F, Si-18F, Al-18F, and C-18F Radiofluorination via Spirocyclic Iodonium Ylides. Journal of Nuclear Medicine 2018, 59 (4), 568–572. [PubMed: 29284673]
30. Wright JS; Kaur T; Preshlock S; Tanzey SS; Winton WP; Sharninghausen LS; Wiesner N; Brooks AF; Sanford MS; Scott PJH, Copper-mediated late-stage radiofluorination: five years of impact on preclinical and clinical PET imaging. Clinical and Translational Imaging 2020, 8 (3), 167–206. [PubMed: 33748018]
31. Mossine AV; Brooks AF; Ichiishi N; Makaravage KJ; Sanford MS; Scott PJH, Development of Customized [18F]Fluoride Elution Techniques for the Enhancement of Copper-Mediated Late-Stage Radiofluorination. Scientific Reports 2017, 7 (1), 233. [PubMed: 28331174]
32. Haka MS; Kilbourn MR; Leonard Watkins G; Toorongian SA, Aryltrimethylammonium trifluoromethanesulfonates as precursors to aryl [18F]fluorides: Improved synthesis of [18F]GBR-13119. Journal of Labelled Compounds and Radiopharmaceuticals 1989, 27 (7), 823–833.
33. Bowden GD; Pichler BJ; Maurer A, A Design of Experiments (DoE) Approach Accelerates the Optimization of Copper-Mediated 18F-Fluorination Reactions of Arylstannanes. Scientific Reports 2019, 9 (1), 11370. [PubMed: 31388076]

Highlights

- Glycogen synthase kinase 3 (GSK-3) is an enzyme that is dysregulated in cancer and brain health illnesses.
- No suitable fluorine-18 labeled GSK-3 radiotracer for positron emission tomography (PET) exists
- Two oxazole-4-carboxamides were labeled with [^{18}F]fluoride.
- Radiotracers were evaluated in rodents and in non-human primate showing good brain uptake.
- [^{18}F]OCM-49 and [^{18}F]OCM-50 are the most promising tracers for imaging of GSK-3 in the brain

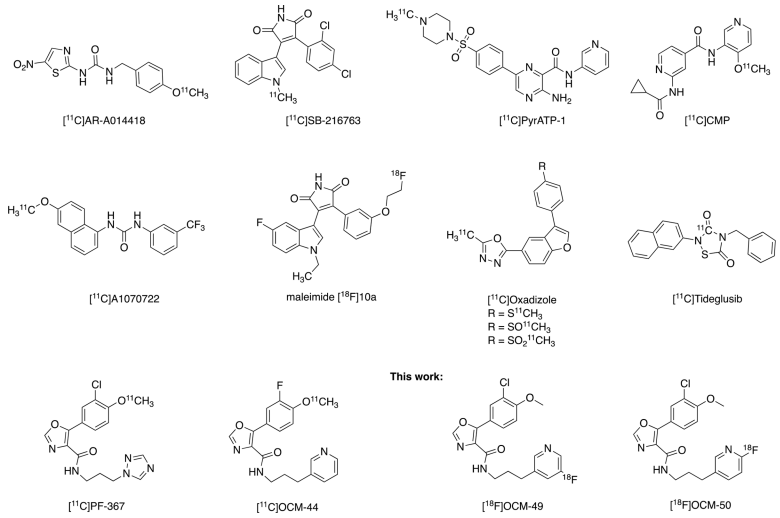

Figure 1.
PET Radiotracers for Imaging GSK-3.

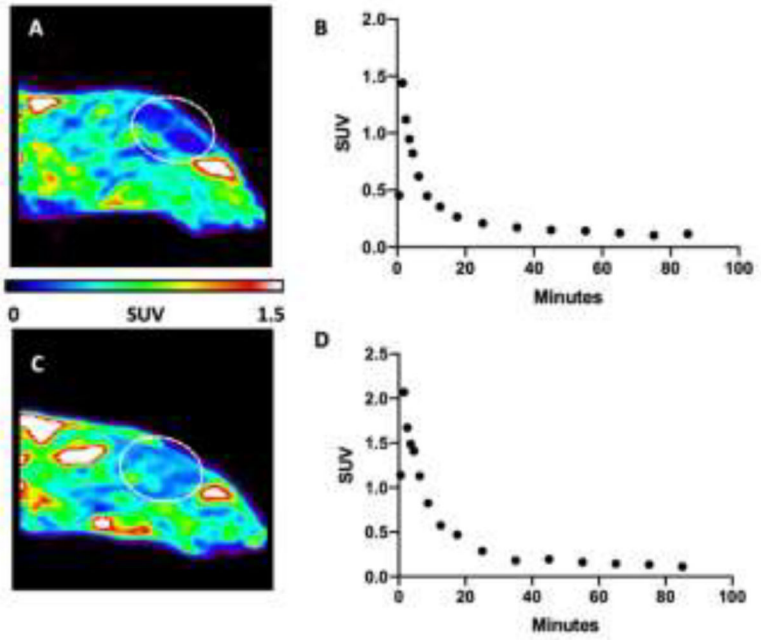

Figure 2. Preclinical PET Imaging with [^{18}F]OCM-49 and [^{18}F]OCM-50 in Rodent.

A) Sagittal summed image (0–90 min) of [^{18}F]OCM-49 PET imaging in Sprague Dawley rat. **B)** Representative whole brain time activity curve (TAC) following *i.v.* administration of [^{18}F]OCM-49. **C)** Sagittal summed image of [^{18}F]OCM-50 PET imaging in Sprague Dawley rat. **D)** Representative regional brain TAC highlighting whole brain uptake and retention following *i.v.* administration of [^{18}F]OCM-50. Dashed white lines depict the brain.

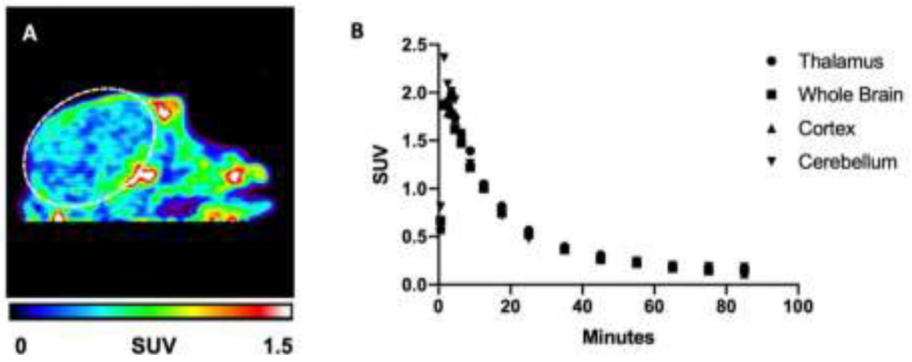

Figure 3. Pre-clinical PET Imaging with [^{18}F]OCM-50 in NHP.

A) Sagittal summed image (0–90 min) of [^{18}F]OCM-50 PET imaging in rhesus monkey. **B)** Thalamus, whole brain, cortex and cerebellum TACs following *i.v.* administration of [^{18}F]OCM-50. Dashed white lines depict the brain.

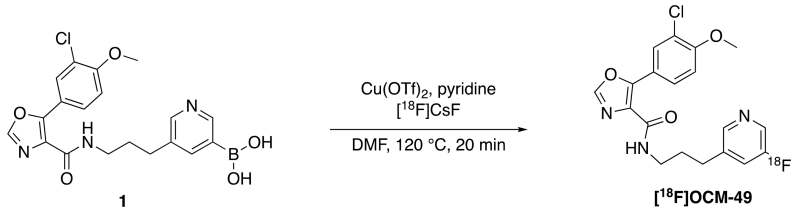

Scheme 1.
Synthesis of [^{18}F]OCM-49.

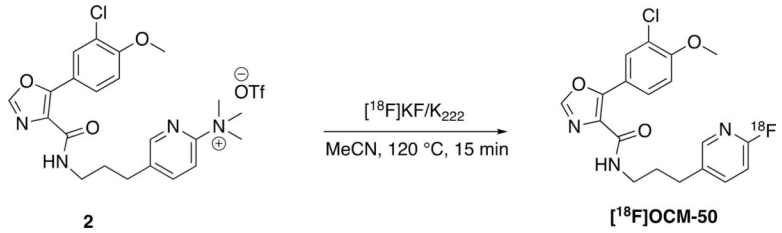

Scheme 2.
Synthesis of [^{18}F]OCM-50.